Article

Effects of Boron Addition on the Microstructure and Mechanical Properties of (Ti,Ta)(C,N)-Co Based Cermets

Ernesto Chicardi [1,*] **and Francisco José Gotor Martínez** [2]

[1]   Department of Engineering and Materials Science and Transport, University of Seville, 41092 Seville, Spain
[2]   Materials Science Institute of Seville (CSIC-US), 41092 Seville, Spain
*   Correspondence: echicardi@us.es; Tel.: +34-954-482-279

check for updates

Abstract: In this work, a titanium–tantalum carbonitride based cermet, with cobalt as the binder phase and boron as a sintering additive, was developed by a mechanically induced self-sustaining reaction process using two different methodologies. The boron additive was added to prevent the formation of brittle intermetallic compounds generally formed during the liquid phase sintering step due to the excessive ceramic dissolution into the molten binder phase. A systematic study was carried out to understand the effects of boron addition on the nature of the phases, microstructure, and mechanical properties of cermets. With the boron addition, the formation of two different boride solid solutions, i.e., $(Ti,Ta)B_2$ and $(Ti,Ta)_3B_4$, was observed. Moreover, the nature of the binder was also modified, from the $(Ti,Ta)Co_2$ brittle intermetallic compound (for cermets without boron addition) to ductile and tough $(Ti,Ta)Co_3$ and α-Co phases (for cermets with boron addition). These modifications caused, as a general trend, the increase of hardness and toughness in cermets.

Keywords: titanium carbonitride; cermet; boron; intermetallic; binder; MSR; powder metallurgy

1. Introduction

Titanium carbonitrides (TiCN) based cermets are potential ceramic-metal composite materials to replace WC-Co hard metals used in the machining industry, in particular, for high speed semi-finishing and finishing work operations [1,2]. These interesting applications are possible thanks to the fact that TiCN-based cermets exhibit high hardness at high temperatures, good thermal stability, relatively high thermal and electrical conductivities, and excellent creep and wear resistances, among other properties [3,4]. However, cermets show poor toughness and damage tolerance compared to hard metals, which must be clearly improved [5].

Current routes used to improve the mechanical properties of cermets are related to the modification of the microstructure and/or composition by the introduction of secondary carbides of transition metals (TaC, TaN, NbC, NbN, VC, etc.), ultrafine- or nano-Ti(C,N) powders, and/or different metallic elements (Co, Ni, Fe, and their alloys, Mo, high entropy alloys, etc.). For example, the introduction of Mo and VC improves the sinterability and hinders the increase in particle size and, consequently, the density, hardness, and mechanical strength is enhanced [6–9]. The addition of ZrC slightly increases the toughness and thermal shock resistance [10], while the introduction of Ni in the binder phase improves the toughness of cermets, but with a small decrease in hardness [11]. Additionally, the introduction of Ta in both the ceramic and binder phases causes a marked improvement in oxidation resistance [12–14].

The use of solid solution carbonitrides as the raw ceramic material has also been proposed to improve the mechanical properties of cermets. These solid solutions are frequently obtained by the combined carbothermal reduction and nitridation of a mixture constituted by the main titanium

oxide component and the secondary transition metal oxides [15–17]. However, this method has some disadvantages, such as the high temperature and the intermediate steps required to synthesize them. In addition, the as-obtained complex solid solution carbonitrides present large particle size that need to be reduced by milling and mixing with the corresponding metallic binder phase. All these aspects add complexity to the powder metallurgical manufacturing process of cermets.

Recently, a new, simple, affordable, and reproducible mechanochemical method, denoted as mechanically induced self-sustaining reaction (MSR), has been successfully applied for the synthesis of complex solid solution carbonitrides with optimal stoichiometric control [18,19] and the development of cermets based on them. The MSR method is a reactive milling process that uses the exothermic nature of the carbonitride formation to synthesize them from the mixture of transition metal elements and a carbon source (usually graphite) under a reactive N_2 atmosphere. However, for the development of the titanium carbonitride based cermets, the use of these highly-activated synthesized powders causes an excessive dissolution of the ceramic particles in the molten metallic binder during the liquid phase sintering step, inducing the formation of intermetallic compounds that act as the binder phase instead of the original Co and/or Ni. Although ductile intermetallic phases have been proposed as interesting candidates for binder in cermets [20], the presence of other brittle intermetallic compounds, such as those corresponding to the Ti-Ta-Co system, can seriously deteriorate the cermets properties, mainly the fracture strength and toughness [21].

To solve the excessive dissolution of the ceramic particles during sintering, an interesting approach based on the introduction of elemental carbon as an additive in the powdered cermets has already been employed. This addition modifies the carbon activity during sintering and reduces the dissolution of the solid solution carbonitride phase into the molten binder phase. This method avoids the formation of brittle intermetallic compounds, improving the toughness of the final cermets [22]. However, as an undesirable effect, the hardness of cermets decreased due to the formation of a soft and ductile binder phase.

In this work, we present another complementary way to reduce or avoid the formation of brittle intermetallic compounds based on the introduction of boron as an additive to react with the dissolved Ti and Ta during sintering. A complete study was carried out to understand the effects caused by the boron addition on the phases formed, the microstructure, and the mechanical properties of the developed cermets.

2. Experimental Procedure

2.1. Development of Cermets

Titanium metal powder (CAS number 7440-32-6, 99.6% purity, <325 mesh, Strem Chemicals, MA, USA), tantalum metal powder (CAS number 7440-25-7, 99.9% purity, <325 mesh, Strem Chemicals), cobalt metal powder (CAS number 7440-48-4, 99.9% purity, <325 mesh, Strem Chemicals), boron amorphous powder (CAS number 7440-48-2, 98% purity, <2 microns, Sigma-Aldrich), graphite powder (CAS number 7782-42-5, 99% purity, <50 microns, Strem Chemicals), and N_2 (H_2O and O_2 63 ppm, Air Liquide, Madrid, Spain) were used as raw materials to develop the titanium carbonitride based cermets with boron addition.

Two set of (Ti,Ta)(C,N) - 20 wt.% Co - (0–2 wt.%) B cermets were developed by two different methodologies, which are schematized in Figure 1. In the first one (Figure 1a), the hard-ceramic component of cermets, with nominal composition of $Ti_{0.8}Ta_{0.2}C_{0.5}N_{0.5}$, was synthesized in situ by MSR from the elemental mixture and mixed with the desired amount of the cobalt metal binder phase in a single milling step. Subsequently, in a second milling step, the boron was added to the powdered cermet previously produced. In the second methodology (Figure 1b), the carbonitride phase with the same nominal composition ($Ti_{0.8}Ta_{0.2}C_{0.5}N_{0.5}$) was first obtained by MSR. Next, in a second milling step, it was mixed with both the cobalt binder phase and the boron additive.

The MSR process in both methodologies was carried out using a modified planetary ball mill (Pulverisette 4, Fritsch, Idar-Oberstein, Germany). Fifty grams of a mixture of the elemental Ti, Ta, Co (this last only for the first methodology), and graphite in the desired stoichiometric ratio were

placed in a 300 mL tempered steel vial (67HRC) together with 15 tempered steel balls (67HRC, 20 mm of diameter and 32.6 g per ball). The powder-to-ball mass ratio (PBR) was 1:9.8. The powder mixtures were milled under 6 atm of high-purity N_2 gas at a spinning rate of 400 rpm for both the rotation of the supporting disc and the superimposed rotation of the vials in the opposite direction. The milling processes were monitored by continuously measuring the pressure inside the vial. When the self-propagating reaction associated with the formation of the hard carbonitride ceramic phase occurred, the temperature increased due to the release of heat from the exothermic reaction, which consequently increased the total pressure. The ignition time (t_{ig}), defined as the critical milling time required to induce the MSR process, could then be determined from the spike in the recorded time–pressure data. Once ignition occurred, the milling was continued for 30 min to ensure full conversion and homogenization. Note that the gas pressure measurement was possible by connecting the vial to a gas cylinder via a rotating union (model 1005-163-038, Deublin, Waukegan, IL, USA) and a flexible polyamide tube and monitoring it by a pressure transducer (AKS, Danfoss, Nordborg, Denmark) connected to a paperless recorder (Ecograph T RSG35, Endress + Hauser, Reinach, Switzerland).
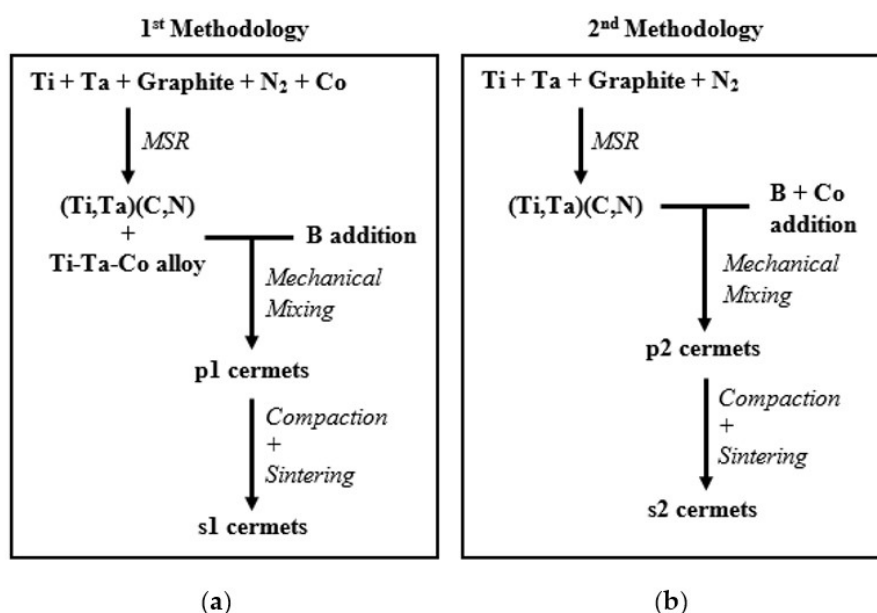

Figure 1. Representative schemes of the two methodologies (**a**,**b**) used to develop the corresponding sets of (Ti,Ta)(C,N)-Co-B based cermets.

After the MSR reaction, the powdered cermet produced in the first methodology or the hard ceramic phase ($Ti_{0.8}Ta_{0.2}C_{0.5}N_{0.5}$), synthesized following the second methodology, were mixed in a planetary mill (Pulverisette P7, Fritsch, Idar-Oberstein, Germany) with 0.5 and 2 wt.% of boron (Figure 1a) or 20 wt.% of Co and 0.5 and 2 wt.% of boron (Figure 1b). A total of 6 g of the mixtures together with 7 tempered steel balls ($\varnothing = 15$ mm, $m = 13.7$ g), PBR of 1:16, were milled at 400 rpm in a 45 mL tempered steel vial (67HRC) under 6 atm of high-purity He gas ($H_2O < 3$ ppm, $O_2 < 2$ ppm, and $C_nH_m < 0.5$ ppm, Air Liquide). The (Ti,Ta)(C,N) - 20 wt.% Co - (0–2 wt.%) B powdered cermets were named as **p***x***B***y*, being "*x*" the methodology used (according to Figure 1a,b) and "*y*" the weight % of boron added (0, 0.5, and 2 wt.%).

The powdered cermets were compacted by uniaxial pressing at 15 MPa for 5 min and cold isostatic pressing at 200 MPa for 10min to yield cylinders of 13 mm in diameter and 9 mm in height. The green compacts were finally sintered at an optimized temperature of 1550 °C for 60 min (heating and cooling rates of 5 °C/min), under flowing Ar in a horizontal tubular furnace (AGNI Type IGM1360 model no. RTH-180-50-1H, AGNI). The label used for the sintered cermets was analogous to the powdered

cermets, replacing the "p" prefix with the "s" prefix, i.e., **s*x*B*y***, "*x*" again being the methodology used and "*y*" the boron weight %.

2.2. Chemical, Microstructural, and Physical Characterization

X-ray diffraction (XRD) patterns were obtained with a X'Pert Pro instrument (Malvern Panalytical, Malvern, UK) equipped with a θ/2θ goniometer using Cu Kα radiation (40 kV, 40 mA), a secondary Kβ filter, and an X'Celerator detector (Malvern Panalytical, Malvern, UK). The diffraction patterns were scanned from 20° to 140° (2θ) in a step-scan mode at a step of 0.02° and a counting time of 275 s/step. Silicon powder (Standard Reference Material 640c, NIST, Gaithersburg, MD, USA) was used for calibration of the diffraction line positions. The space group symmetry (SGS) as well as the lattice parameters of phases were calculated from the whole set of peaks of the XRD pattern by the free DICVOL06 software, which uses the dichotomy method for powder pattern indexing. The elucidated structures were compared with those in the PDF-4+ database from the International Centre for Diffraction Data (ICDD).

Scanning electron microscopy (SEM) images of the sintered cermets were recorded on a S-4800 field emission SEM instrument (Hitachi, Tokio, Japan) in secondary electron mode at an acceleration voltage of 5 kV. The morphology, structure, distribution, and homogeneity of phases in cermets were studied. SEM images at different magnifications (1000×, 2000×, and 5000×) were recorded to evaluate the volume percentage of the ceramic, the binder, and the porosity (Vc, Vb, and ρ, respectively) and the particle size average and distribution (d) by Image Analysis (IA) using Image-Pro Plus 6.2 software (Media Cybernetics, Rockville, MD, USA). The Ti, Ta, and Co amounts were measured by X-ray energy dispersive spectrometry (EDS, Hitachi, Tokio, Japan), using a detector coupled with SEM at an acceleration voltage of 30 kV. For each sintered cermet, around 30 point measurements were performed. In addition, EDS-SEM mappings were performed under the same experimental conditions.

2.3. Mechanical Behavior

Hardness measurements were carried out on polished surfaces at an indentation load of 5 kgf (HV5) using a Zwick 3212 Vickers diamond pyramidal indenter (ZwickRoell, Barcelona, Spain)). No artefacts from the indentation load effect were observed at 5 kgf. The indentation time was 15 s. Ten indentations were made for each sintered cermet.

The fracture toughness, K_{Ic}, was evaluated by the indentation microfracture (IM) method using the crack length produced at the corners of Vickers indentations and the equation derived from Shetty et al. [23]:

$$K_{Ic} = 0.0319 \cdot P/(a \cdot l^{1/2}),$$

where P denotes the load (N), a is the half of the indentation diagonal (m), and l is the crack length measured from the vertices of the indentation to the crack tip (m). This method has been proven to give reasonable estimates of K_{Ic} in cemented carbides up to values of approximately 15 MPa·m$^{1/2}$ with maximum deviations of 20%, compared to fracture toughness data obtained from single-edge-notched-beam specimens [24]. A load of 50 kgf was used to produce cracks with at least half the length of the indentation diagonal, which is the minimum length required to obtain K_{Ic} values independent of the load [25]. Accurate measurements of crack lengths were made using the above-mentioned scanning electron microscope.

3. Results and Discussion

3.1. Synthesis of the Powdered Cermets with Boron Addition

The XRD patterns of the powders obtained after the MSR process and previous to sintering are shown in Figure 2. For the first methodology, the three powdered cermets (**p1B0**, **p1B0.5**, and **p1B2**) showed the formation of a titanium–tantalum carbonitride solid solution (Ti,Ta)(C,N) with a cubic structure and Fm3m SGS, as observed in a previous work using the same methodology [26]. This statement was made by comparison with the reference patterns TiN (38-1420), TiC (32-1383),

TaC (35-0801), and TaN (49-1283) in the PDF-4+ database from ICDD. Additionally, in Reference [26], electron diffraction (ED) and XEDS measurements corroborated the existence of the solid solution. A small "hump" at ~43° 2θ was also observed for the three powdered cermets, which was attributed to a partially amorphized Co-Ti-Ta alloy, according to a previous work [21].
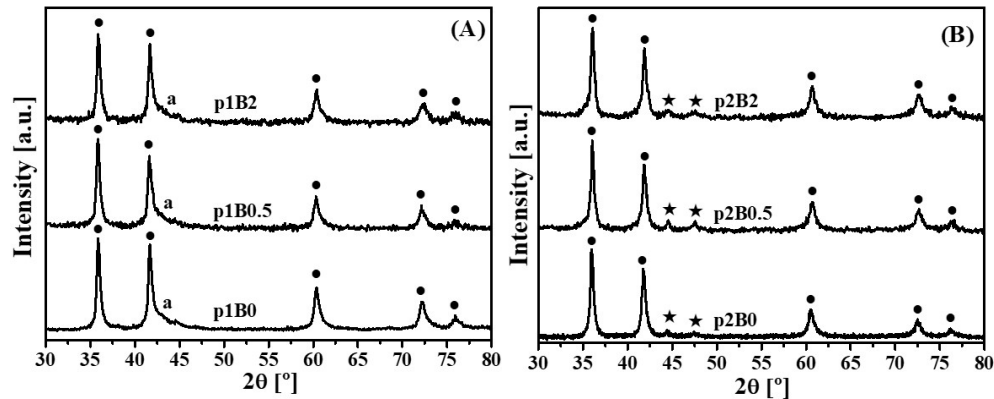

Figure 2. X-ray diffraction patterns of the powdered (Ti,Ta)(C,N)-Co-B based cermets. (**A**) First methodology (**p1B0**, **p1B0.5**, and **p1B2**), (**B**) second methodology (**p2B0**, **p2B0.5**, and **p2B2**), (●) (Ti,Ta)(C,N) (Fm3m), (**a**) amorphized Co-Ti-Ta alloy, and (★) Co (P63/mmc).

The powdered cermets developed by the second methodology, (**p2B0**, **p2B0.5**, and **p2B2**) showed the same titanium–tantalum carbonitride solid solution (Ti,Ta)(C,N) as for the first methodology [2]. However, the XRD peaks corresponding to the Co binder phase, which was added for the second milling step, were clearly observed. In this case, the presence of the "hump" was not detected and suggested that the Co-Ti-Ta alloy above-mentioned was formed as a result of the heat release during the formation of the carbonitride phase by the MSR reaction. Note the different nature of the binder phases obtained by both methodologies, which may have significance in the phases developed after the sintering process and, consequently, in the mechanical properties.

3.2. Sintering of Cermets with Boron Addition

The XRD patterns of sintered cermets are shown in Figure 3. For the first methodology, although the XRD patterns showed the already mentioned titanium–tantalum carbonitride solid solution, (Ti,Ta)(C,N), as the major ceramic phase, significance differences were observed between the three sintered cermets (**s1B0**, **s1B0.5**, and **s1B2**). For the cermet without boron addition (**s1B0**), a (Ti,Ta)Co$_2$ intermetallic phase with a cubic structure (SGS Fd3m), acting as the binder phase instead of the starting elemental Co, was indexed. This phase was reported in a previous work and corresponds to an intermetallic solid solution between TiCo$_2$ (ref. No. 017-0031) and TaCo$_2$ (ref. No. 038-0736) [26]. However, when 0.5 wt.% of boron was added in the second milling step, the XRD pattern ostensibly changed. The XRD peaks corresponding to (Ti,Ta)Co$_2$ decreased sharply, suggesting that their percentage diminished when B was added. In addition, another three different phases were detected that could be indexed to another intermetallic compound with a higher amount of cobalt, (Ti,Ta)Co$_3$ (cubic structure, SGS Pm3m), a solid solution of TiCo$_3$ (ref. No. 023-0938), and TaCo$_3$ (ref. No. 015-0028), and other two ceramic phases containing boron, (Ti,Ta)B$_2$ and (Ti,Ta)$_3$B$_4$, with hexagonal (SGS P6/mmm) and orthorhombic (SGS Immm) structures, respectively. They are solid solutions in the TiB$_2$ (ref. No. 035-0741) - TaB$_2$ (ref. No. 038-1462) and Ti$_3$B$_4$ (ref. No. 019-1368) - Ta$_3$B$_4$ (ref. No. 047-1529) systems, respectively. Therefore, the introduction of boron caused the reaction of this element with titanium and tantalum to form boride ceramic phases during sintering, decreasing the final Ti and Ta content in the binder phase, which evolved from 1:2, (Ti,Ta)Co$_2$, to 1:3, (Ti,Ta)Co$_3$, stoichiometry. This trend of reducing Ti and Ta in the binder was corroborated when 2 wt.% of boron was added. In this case (Figure 3), not only was the (Ti,Ta)Co$_3$ intermetallic observed, but also the α-Co alloy (cubic structure

and Fm3m). Moreover, the remnant (Ti,Ta)Co$_2$, with a probably modified Ti/Ta ratio, changed from a cubic to a hexagonal structure (SGS P6/mmm). Obviously, the peaks corresponding to the boride phases slightly increased due to the higher amount of boron introduced in the **s1B2** cermet.
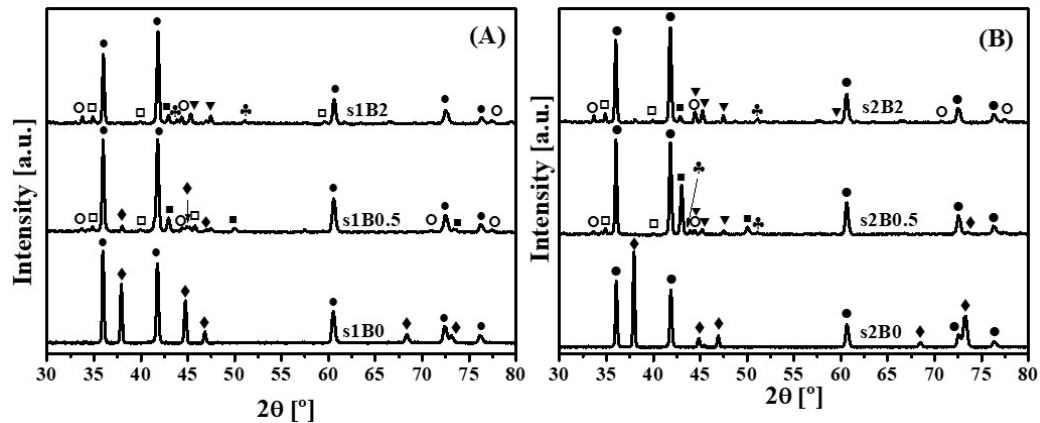

Figure 3. X-Ray Diffraction patterns of the sintered (Ti,Ta)(C,N)-Co-B based cermets. (**A**) First methodology (**s1B0**, **s1B0.5**, and **s1B2**), (**B**) second methodology (**s2B0**, **s2B0.5**, and **s2B2**), (●) (Ti,Ta)(C,N) (Fm3m), (◆) (Ti,Ta)Co$_2$ (Fd3m), (▼) (Ti,Ta)Co$_2$ (P63/mmc), (■) (Ti,Ta)Co$_3$ (Pm3m), (♣) α-Co (Fm3m), (○) (Ti,Ta)B$_2$ (P6/mmm), and (□) (Ti,Ta)$_3$B$_4$ (Immm).

For the second methodology, the XRD patterns of the sintered cermets (**s2B0, s2B0.5**, and **s2B2**) showed analogous phases to those observed in the first methodology. The unique different aspect was the detection of the α-Co alloy, even when only a 0.5 wt.% of boron was added, in contrast with the first methodology, when this phase was detected for 2 wt.% of boron (**s1B2**). Note the absence of Ti and Ta prior to sintering in the binder phase, unlike what happened with the first methodology. Therefore, boron reacted directly with Ti and Ta dissolved from the ceramic particles during sintering, forming the corresponding boride phases, i.e., the (Ti,Ta)B$_2$ and (Ti,Ta)$_3$B$_4$. Obviously, when the boron was consumed as a result of these reactions, the excess of Ti and Ta dissolved into the molten binder phase caused the formation of hexagonal (Ti,Ta)Co$_2$ and cubic (Ti,Ta)Co$_3$ intermetallic compounds.

SEM images of all sintered cermets are displayed in Figure 4. In these images, it is possible to observe the typical core-rim microstructure for the (Ti,Ta)(C,N) ceramic phase in cermets obtained from the first methodology and the practical absence of this ceramic microstructure in those obtained from the second methodology. This aspect has already been corroborated for the authors in two previous works [2,26]. EDS point analyses (Table 1) performed in the ceramic phases (marked as points 1 (core) and 2 (rim) in s1 cermets and 3 in s2 cermets of Figure 4) corroborated that they are a double Ti-Ta carbonitride solid solution. The composition of (Ti,Ta)(C,N) in s2 cermets matched with the core in s1 cermets. It was confirmed that the rim phase in s1 cermets was richer in Ti than the core phase, in agreement with Reference [26]. On the other hand, the binder phases showed different contrasts in the SEM images, especially in cermets containing boron, suggesting that they are composed of different metallic phases as indexed by XRD. The EDS point analyses performed in the binder phases (points 4, 5, and 6 in cermets s1 and 7, 8, 9, and 10 in cermets s2) were in agreement with the presence of (Ti,Ta)Co$_2$ and (Ti,Ta)Co$_3$ intermetallics and α-Co alloy. The slightly different chemical compositions found for the (Ti,Ta)Co$_2$ intermetallic from EDS results (Table 1) may be related to the different structure observed in XRD, since Co–Ta and Co–Ti phase diagrams suggest that the hexagonal structure is preferentially formed over the cubic structure for slightly higher Co compositions. Finally, point EDS analyses on the dark faceted particles detected in cermets with boron addition, i.e., the **s1B0.5, s1B2, s2B0.5**, and **s2B2** (marked as number 11 in Figure 4), showed a really high Ti composition, a small amount of Ta, and the total absence of C and N. Thus, this phase was attributed to the borides detected by XRD. It was impossible to discriminate between (Ti,Ta)B$_2$ and (Ti,Ta)$_3$B$_4$ due to a similar stoichiometry and the absence of a B signal in EDS analysis.
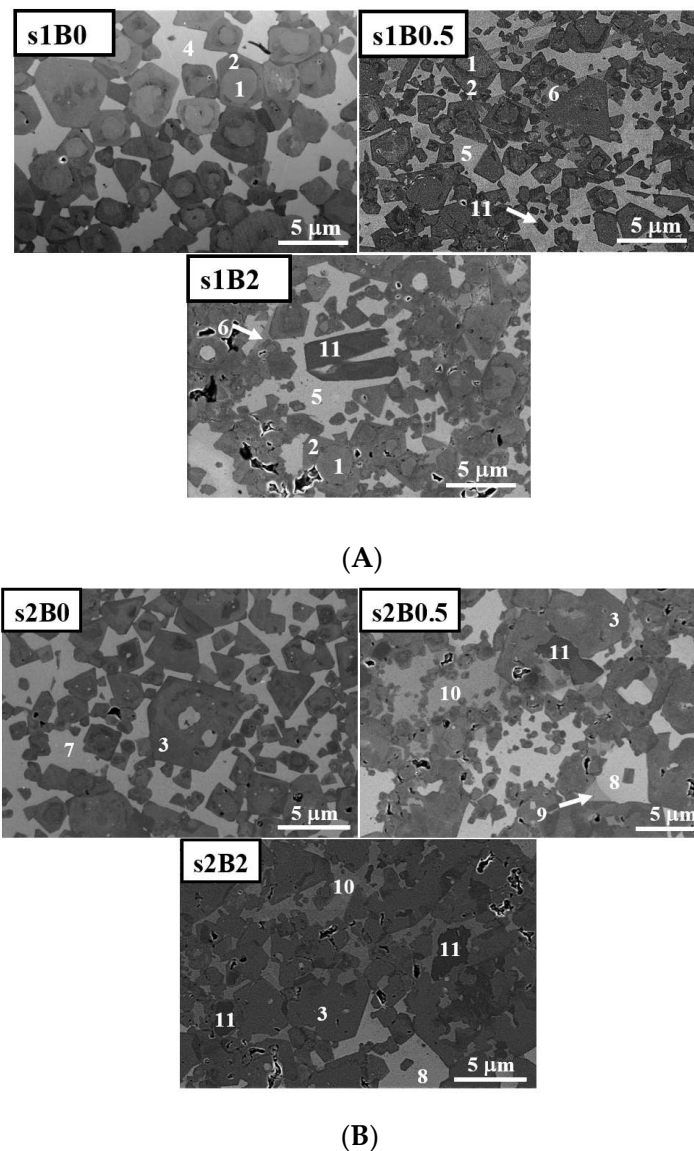
(A)

(B)

Figure 4. Secondary Scanning Electron Microscopy (SEM) images of the sintered (Ti,Ta)(C,N)-Co-B cermets obtained by: (**A**) The first methodology (**s1B0**, **s1B0.5**, and **s1B2**) and (**B**) the second methodology (**s2B0**, **s2B0.5**, and **s2B2**). The numbers in the images correspond to the composition phases shown in Table 1.

Table 1. Semiquantitative transition metals composition (Ti, Ta, and Co) in atomic percentage (at. %) for both sets of (Ti,Ta)(C,N)-Co-B based cermets: **s1B0**, **s1B0.5**, **s1B2**, **s2B0**, **s2B0.5**, and **s2B2**.

Area	Atomic Percentage (at. %)			Phase
	Ti	**Ta**	**Co**	**-**
1	83.4 ± 2.1	16.6 ± 2.1	-	(Ti,Ta)(C,N)-core
2	86.8 ± 1.3	13.2 ± 1.3	-	(Ti,Ta)(C,N)-rim
3	83.8 ± 0.5	16.2 ± 0.5	-	(Ti,Ta)(C,N)
4	21.5 ± 1.0	10.0 ± 1.0	68.5 ± 1.0	$(Ti,Ta)Co_2$
5	21.1 ± 1.2	15.3 ± 1.2	63.8 ± 1.2	$(Ti,Ta)Co_2$
6	16.7 ± 0.8	8.1 ± 0.8	75.2 ± 0.8	$(Ti,Ta)Co_3$
7	18.4 ± 1.4	12.7 ± 1.4	68.9 ± 1.4	$(Ti,Ta)Co_2$
8	15.3 ± 1.0	20.2 ± 1.0	64.5 ± 1.0	$(Ti,Ta)Co_2$
9	14.7 ± 1.7	10.0 ± 1.7	75.3 ± 1.7	$(Ti,Ta)Co_3$
10	12.4 ± 0.7	2.2 ± 0.7	85.4 ± 0.7	-Co
11	96.5 ± 1.1	3.5 ± 1.1	-	$(Ti,Ta)B_2$ or $(Ti,Ta)_3B_4$.

On the other hand, EDS mapping in the s2B2 cermet was made to verify the distribution of phases observed by XRD in a qualitative way (Figure 5). The high content of Ti (red color) in the ceramic phase, (Ti,Ta)(C,N), easily allowed its identification. The brightness of the Ta map (green color) in the ceramic phase was lower due to its lower amount, the nominal Ti/Ta ratio was equal to 4 (Ti0.8Ta0.2). In addition, the N (orange color) and C (purple color) maps were always associated with this phase, confirming the formation of the carbonitride phase. Note that the high carbon brightness observed in the zone marked with a white circle is an artefact caused by the presence of porosity in this area. As opposite, the Ta brightness was higher in the area where Co was present, corroborating the Ta presence in the binder phase. It is necessary to comment that, although Ti was also in the binder phase, its contrast was practically negligible due to the different Ti amount with respect to the carbonitride phase. Additionally, related to the Co (light blue color) map, three different brightness are observed, marked as white squares with continuous lines in Figure 5. They correspond to the three binder phases detected by XRD and point to EDS carried out in those areas, i.e., $(Ti,Ta)Co_2$, $(Ti,Ta)Co_3$, and α-Co. Finally, dark particles, marked with white squares with dotted lines, showed a high amount of Ti and B, suggesting they are the boride phases formed during sintering.
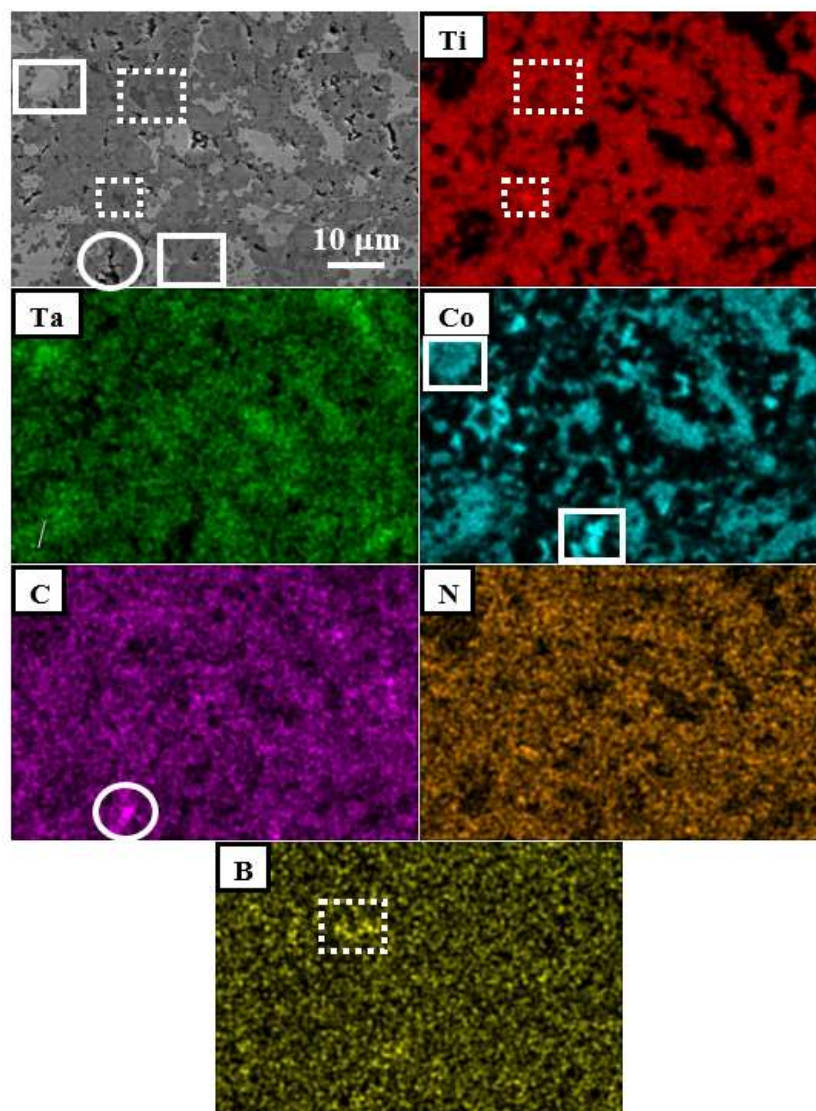

Figure 5. Energy-dispersive X-ray spectroscopy (EDS) mapping of the **s2B2** sintered cermet. Continuous line squares: The three binder phases detected, i.e., $(Ti,Ta)Co_2$, $(Ti,Ta)Co_3$, and α-Co. Dotted line squares: Boride phases, i.e., $(Ti,Ta)B_2$ and/or $(Ti,Ta)_3B_4$. Circles: Artefacts caused by the porosity.

3.3. Physical and Mechanical Properties of Sintered Cermets.

The porosity of the sintered cermets, measured by image analysis (Table 2), showed similar values for all of them. Porosity of around 2–3 vol.% was determined. Only, for the **s1B0** sintered cermet, a slightly higher value of around 4 vol.% was calculated. This fact could suggest that the presence of Ti and, particularly, Ta, with a high melting point, in the binder phase in cermets developed by the first methodology prior to sintering, negatively affected the consolidation step. However, when B was added, the formation of the borides decreased the Ti and Ta into the binder phase, diminishing their harmful behaviour.

Table 2. Physical characteristics (volumetric porosity (ρ), average ceramic particle size (d), volumetric binder phase percentage (Vb), and mechanical properties (Vickers hardness (HV) and fracture toughness (K_{IC})) for both sets of (Ti,Ta)(C,N)-Co-B based cermets: **s1B0**, **s1B0.5**, **s1B2**, **s2B0**, **s2B0.5**, and **s2B2**.

Cermet	d (μm)	Vb (vol.%)	ρ (vol.%)	HV (GPa)	K_{IC} (MPa·m$^{1/2}$)
s1B0	1.7 ± 0.3	26 ± 3	4.0 ± 0.6	11.9 ± 1.2	4.0 ± 0.6
s1B0.5	1.5 ± 0.5	21 ± 3	1.6 ± 0.5	12.9 ± 0.8	3.6 ± 1.0
s1B2	1.4 ± 0.3	23 ± 2	2.6 ± 1.1	12.8 ± 0.5	4.0 ± 0.5
s2B0	3.1 ± 0.5	28 ± 2	2.2 ± 0.5	14.1 ± 1.0	2.9 ± 0.3
s2B0.5	2.8 ± 0.4	26 ± 2	3.4 ± 0.8	14.0 ± 1.0	5.3 ± 1.0
s2B2	2.4 ± 0.3	26 ± 3	2.8 ± 0.7	16.2 ± 0.8	3.3 ± 0.9

On the other hand, larger (Ti,Ta)(C,N) ceramic particles were observed in s2 cermets than in s1 cermets. The particle size values determined from SEM images are also shown in Table 2. This aspect is the direct consequence of the dissolution–reprecipitation of the ceramic phase as the main sintering mechanism in cermets obtained by the first methodology (**s1B0**, **s1B0.5**, and **s1B2**), while the coalescence of the ceramic particles was also observed in s2 cermets. Another interesting physical characteristic determined by image analysis was the percentage of binder phase (Table 2). A slight decrease of the binder phase percentage when boron was added was observed. This fact was attributed to the formation of the new boride ceramic phases, consequently reducing the amount of Ti and Ta in the Co-containing binder phase. These two aspects can influence the mechanical properties of cermets developed with boron addition.

Concerning the mechanical properties, as a general trend, the hardness of cermets increased with the boron addition, presumably due to the formation of the new boride hard phases. The hardness improvements reached a 15% for cermet **s2B2,** compared to **s2B0**. In **s2B0.5** cermet, the opposite effects of the boride formation and the development of less hard binder phases (($Ti,Ta)Co_3$ and α-Co) induced a similar hardness value than the corresponding cermet without boron (**s2B0**). In addition, the slight hardness increase of the s2 cermets, compared to s1 cermets, could be attributable to the absence of the core-rim structure in the first ones, due to the microstructural misfit between the core and the rim [27], which can produce internal stress and damage the mechanical properties.

In turn, the fracture toughness, measured by the indentation method, remained practically invariant when boron was added. Thus, although the new binder phases formed when boron was added (($Ti,Ta)Co_3$ and α-Co) are more tough than ($Ti,Ta)Co_2$, formed without boron addition, the decrease of the binder phase amount counteracted this effect [28]. Only the cermet **s2B0.5** showed a significant increase of fracture toughness with the boron addition, due to the major tough ($Ti,Ta)Co_3$ binder phase, as observed by XRD (see Figure 3). By contrast, the fracture toughness of **s2B2** decreased. This contrary behavior was attributable to the higher boride phases (($Ti,Ta)B_2$ and $(Ti,Ta)_3B_4$) formed, which reduce the Ti and Ta in the binder phase, in detriment of the ($Ti,Ta)Co_3$ formation.

4. Conclusions

A systematic study of the effect of boron addition on titanium–tantalum carbonitride based cermets, developed by MSR process and using two different methodologies, was carried out. The following conclusions can be made:

(1) The addition of boron to (Ti,Ta)(C,N)-Co based cermets during the sintering step caused the formation of two different boride solid solutions, i.e., $(Ti,Ta)B_2$ and $(Ti,Ta)_3B_4$.

(2) The main mechanism of this process seems to be different for both methodologies. While for the first methodology the boron mainly reacts with the Ti and Ta presented in the binder phase prior to the sintering step, for the second methodology, the boron reacted with the Ti and Ta dissolved from the (Ti,Ta)(C,N) ceramic phase.

(3) This reaction of the boride formation allowed for the decrease of the Ti and Ta amounts in the binder phase and, consequently, the modification of the binder nature. Particularly, the $(Ti,Ta)Co_2$ brittle intermetallic compound observed for cermets without boron addition evolved to a new $(Ti,Ta)Co_3$ and α-Co alloy, more ductile and tough than $(Ti,Ta)Co_2$.

(4) As a general trend, the increase of hardness and toughness was due to the formation of new ceramic phases (borides) and tougher and ductile binder phases, respectively.

(5) This new approach for reducing the amount of transition metals (in this case, Ti and Ta) in the binder phase of cermets, based on the reaction with boron to synthesize borides, can be an alternative way to other, already published, approaches focused on reducing the ceramic dissolution during sintering.

Author Contributions: The two authors of this work have contributed to the same extend in all steps, from the conceptualization of the research idea to the final writing.

Conflicts of Interest: The authors declare no conflict of interest.

References

1. Bellosi, A.; Calzavarini, R.; Faga, M.G.; Monteverde, F.; Zancolò, C.; D'Errico, G.E. Characterisation and application of titanium carbonitride-based cutting tools. *J. Mater. Process. Technol.* **2003**, *143–144*, 527–532. [CrossRef]

2. Chicardi, E.; Córdoba, J.M.; Sayagués, M.J.; Gotor, F.J. Absence of the core–rim microstructure in TixTa1−xCyN1−y-based cermets developed from a pre-sintered carbonitride master alloy. *Int. J. Refract. Met. Hard Mater.* **2012**, *33*, 38–43. [CrossRef]

3. Chicardi, E.; Torres, Y.; Córdoba, J.M.; Sayagués, M.J.; Rodríguez, J.A.; Gotor, F.J. Effect of sintering time on the microstructure and mechanical properties of (Ti,Ta)(C,N)-based cermets. *Int. J. Refract. Met. Hard Mater.* **2013**, *38*, 73–80. [CrossRef]

4. Zhang, H.; Yan, J.; Zhang, X.; Tang, S. Properties of titanium carbonitride matrix cermets. *Int. J. Refract. Met. Hard Mater.* **2006**, *24*, 236–239. [CrossRef]

5. De la Obra, G.; Avilés, M.A.; Torres, Y.; Chicardi, E.; Gotor, F.J. A new family of cermets: Chemically complex but microstructurally simple. *Int. J. Refract. Met. Hard Mater.* **2017**, *63*, 17–25. [CrossRef]

6. Chicardi, E.; Gotor, F.J.; Medri, V.; Guicciardi, S.; Lascano, S.; Córdoba, J.M. Hot-pressing of (Ti,Mt)(C,N)–Co–Mo2C (Mt=Ta,Nb) powdered cermets synthesized by a mechanically induced self-sustaining reaction. *Chem. Eng. J.* **2016**, *292*, 51–61. [CrossRef]

7. LaSalvia, J.C.; Kim, D.K.; Meyers, M.A. Effect of Mo on microstructure and mechanical properties of TiC—Ni-based cermets produced by combustion synthesis—Impact forging technique. *Mater. Sci. Eng. A* **1996**, *206*, 71–80. [CrossRef]

8. Wang, J.; Liu, Y.; Zhang, P.; Ye, J.; Tu, M. Effect of VC and nano-TiC addition on the microstructure and properties of micrometer grade Ti(CN)-based cermets. *Mater. Des.* **2009**, *30*, 2222–2226. [CrossRef]

9.   Zhang, G.; Xiong, W.; Yang, Q.; Yao, Z.; Chen, S.; Chen, X. Effect of Mo addition on microstructure and mechanical properties of (Ti,W)C solid solution based cermets. *Int. J. Refract. Met. Hard Mater.* **2014**, *43*, 77–82. [CrossRef]

10.   Zhang, X.; Liu, N. Effects of ZrC on microstructure, mechanical properties and thermal shock resistance of TiC–ZrC–Co–Ni cermets. *Mater. Sci. Eng. A* **2013**, *561*, 270–276. [CrossRef]

11.   Xu, Q.; Ai, X.; Zhao, J.; Gong, F.; Pang, J.; Wang, Y. Effects of metal binder on the microstructure and mechanical properties of Ti(C,N)-based cermets. *J. Alloy. Compd.* **2015**, *644*, 663–672. [CrossRef]

12.   Chicardi, E.; Córdoba, J.M.; Gotor, F.J. High temperature oxidation resistance of (Ti,Ta)(C,N)-based cermets. *Corros. Sci.* **2016**, *102*, 125–136. [CrossRef]

13.   Chicardi, E.; Córdoba, J.M.; Gotor, F.J. Kinetics of high-temperature oxidation of (Ti,Ta)(C,N)-based cermets. *Corros. Sci.* **2016**, *102*, 168–177. [CrossRef]

14.   Chicardi, E.; Gotor, F.J.; Córdoba, J.M. Enhanced oxidation resistance of Ti(C,N)-based cermets containing Ta. *Corros. Sci.* **2014**, *84*, 11–20. [CrossRef]

15.   Kwon, H.; Kim, W.; Kim, J. Stability domains of (Ti,W)C and (Ti,W)(CN) during carbothermal reduction of TiO_2/WO_3 mixture at 1500K. *J. Eur. Ceram. Soc.* **2017**, *37*, 1355–1371. [CrossRef]

16.   Qiu, W.; Liu, Y.; Ye, J.; Fan, H.; Qiu, Y. Effects of (Ti,Ta,Nb,W)(C,N) on the microstructure, mechanical properties and corrosion behaviors of WC-Co cemented carbides. *Ceram. Int.* **2017**, *43*, 2918–2926. [CrossRef]

17.   Zhou, W.; Zheng, Y.; Zhao, Y.; Zhang, G.; Dong, Z.; Xiong, W. Fabrication of Ti(C,N)-based cermets by in situ carbothermal reduction of MoO3 and subsequent liquid sintering. *J. Am. Ceram. Soc.* **2017**, *100*, 1578–1587. [CrossRef]

18.   De la Obra, A.G.; Gotor, F.J.; Chicardi, E. Effect of the impact energy on the chemical homogeneity of a (Ti,Ta,Nb)(C,N) solid solution obtained via a mechanically induced self-sustaining reaction. *J. Alloy. Compd.* **2017**, *708*, 1008–1017. [CrossRef]

19.   Córdoba, J.M.; Avilés, M.A.; Sayagués, M.J.; Alcalá, M.D.; Gotor, F.J. Synthesis of complex carbonitride powders TiyMT1−yCxN1−x (MT: Zr, V, Ta, Hf) via a mechanically induced self-sustaining reaction. *J. Alloy. Compd.* **2009**, *482*, 349–355. [CrossRef]

20.   Alvarez, M.; Sánchez, J.M. Spark plasma sintering of Ti(C,N) cermets with intermetallic binder phases. *Int. J. Refract. Met. Hard Mater.* **2007**, *25*, 107–118. [CrossRef]

21.   Chicardi, E.; Torres, Y.; Córdoba, J.M.; Hvizdoš, P.; Gotor, F.J. Effect of tantalum content on the microstructure and mechanical behavior of cermets based on (TixTa1−x)(C0.5N0.5) solid solutions. *Mater. Des.* **2014**, *53*, 435–444. [CrossRef]

22.   Chicardi, E.; Torres, Y.; Sayagués, M.J.; Medri, V.; Melandri, C.; Córdoba, J.M.; Gotor, F.J. Toughening of complete solid solution cermets by graphite addition. *Chem. Eng. J.* **2015**, *267*, 297–305. [CrossRef]

23.   Coric, D.; Curkovic, L. Statistical analysis of Vickers indentation fracture toughness of Y-TZP ceramics. *Trans. FAMENA* **2017**, *41*, 1–16. [CrossRef]

24.   Spiegler, R.; Schmauder, S.; Sig, L. Fracture toughness evaluation of WC–Co alloys by indentation testing. *J. Hard Met.* **1990**, *1*, 158–174.

25.   Warren, R.; Matzke, H. Indentation Testing of a Broad Range of Cemented Carbides. In *Science of Hard Materials*; Viswanadham, R.K., Rowcliffe, D.J., Gurland, J., Eds.; Springer Publishing: New York, NY, USA, 1983; pp. 563–582.

26.   Chicardi, E.; Córdoba, J.M.; Sayagués, M.J.; Gotor, F.J. Inverse core–rim microstructure in (Ti,Ta)(C,N)-based cermets developed by a mechanically induced self-sustaining reaction. *Int. J. Refract. Met. Hard Mater.* **2012**, *31*, 39–46. [CrossRef]

27.   Ahn, S.Y.; Kim, S.W.; Kang, S. Microstructure of Ti(CN)–WC–NbC–Ni Cermets. *J Am. Ceram. Soc.* **2001**, *84*, 843–849. [CrossRef]

28.   Park, C.; Nam, S.; Kang, S. Enhanced toughness of titanium carbonitride-based cermets by addition of (Ti,W)C carbides. *Mater. Sci. Eng. A* **2016**, *649*, 400–406. [CrossRef]